Experimental Investigation into the Drag Performance of Chevron-Shaped Protrusions in Wall-Bounded Turbulence

Carrasco Grau, Julio; van Campenhout, Olaf W.G.; Hartog, Friso H.; van Nesselrooij, Michiel; Baars, Woutijn J.; Schrijer, Ferdinand F.J.

DOI
10.1007/s10494-023-00451-0

Publication date
2023

Document Version
Final published version

Published in
Flow, Turbulence and Combustion

Flow, Turbulence and Combustion
https://doi.org/10.1007/s10494-023-00451-0

RESEARCH

Experimental Investigation into the Drag Performance of Chevron-Shaped Protrusions in Wall-Bounded Turbulence

Julio Carrasco Grau[1] · Olaf W. G. van Campenhout[1,2] · Friso H. Hartog[1,2] · Michiel van Nesselrooij[1,2] · Woutijn J. Baars[1] · Ferdinand F. J. Schrijer[1]

Received: 10 March 2023 / Accepted: 25 June 2023

Abstract
Chevron-shaped protrusions have been proposed in the literature for turbulent skin friction reduction. However, there is no consensus on the performance of this passive flow control technique; both an increase and a decrease in drag have been observed in previous studies. There is also no experimental evidence to support the working mechanism behind the drag reduction effect that has been postulated in the literature. In this study, direct force measurements were used to replicate experiments from the literature and, in addition, were used to test new array configurations to characterise the effect of individual design parameters on drag performance. A total of 23 different protrusion configurations were investigated in a turbulent boundary layer flow. In addition to the integral force measurements, particle image velocimetry was used to measure wall-parallel velocity fields in order to extract the statistical sizing and energy of the near-wall cycle turbulence. All configurations increased the drag between 2% and 10% for a friction Reynolds number of 1700. The drag reduction reported in the literature could not be replicated; however, these findings agreed with an experimental and numerical study that reported drag increase. The trend observed in the low-speed streak spacing from the PIV experiments was consistent with that observed in the balance data. Nevertheless, no evidence was found to support the working mechanism proposed in the literature. These results cast doubt on the proposed drag reduction potential of chevron-shaped protrusions. In the authors' view, the results of this study strengthen previous conclusions regarding their minor increase in drag. Future studies to further approach a consensus are proposed.

Keywords Protrusions · Chevron · Drag reduction · Turbulent boundary layer · Wind tunnel experiment

✉ Julio Carrasco Grau
juliocarrtud@gmail.com

[1] Faculty of Aerospace Engineering, Delft University of Technology, Kluyverweg 1, 2629 HS Delft, The Netherlands

[2] Dimple Aerospace B.V., Kluyverweg 1, 2629 HS Delft, The Netherlands

Published online: 26 July 2023

1 Introduction

The intuitive belief that smooth surfaces offer optimal performance in terms of minimal drag has been challenged in both laminar and turbulent flow. For instance, transition delay has been studied by Fransson et al. (2006) to reduce drag by using surface bumps; Rius Vidales and Kotsonis (2021) achieved the same effect using forward-facing steps. In the context of turbulent flow, riblets are currently the most researched method for drag reduction (Walsh 1982). Other less well understood but potentially interesting methods for turbulent skin friction reduction are the use of omnidirectional roughness (Tani 1988) and chevron-shaped protrusions (CSP) (Sirovich and Karlsson 1997). Despite the positive results reported in the literature for these methods of flow manipulation, replication has proven to be difficult, indicating the great sensitivity of the results to variations in geometry and flow conditions (Choi 2006).

CSP could offer some key advantages over other passive flow-control techniques. For instance, their large size (compared to riblets) could make protrusions less prone to clogging and, hence, more robust in practical applications. Furthermore, the 10% skin friction reduction reported by Sirovich and Karlsson (1997) would translate into a relevant fuel saving even after considering reductions in effectiveness under operational conditions due to factors such as scaling and non-applicable surfaces, as discussed by Spalart and McLean (2011). Hence, this technique is deemed a relevant topic for further research.

Sirovich and Karlsson (1997) were the first to introduce the concept of CSP. These protrusions have a defined geometry and are arranged in rows as shown in Fig. 1. In this schematic and throughout the rest of the paper, a Cartesian coordinate system is introduced with x, y, and z denoting the streamwise, wall-normal, and spanwise directions, respectively. In the study by Sirovich and Karlsson (1997), the height of these elements (F) was $5-6$ and the width of the element (C) was 200 in near-wall length scale (approximately 100 μm and 3.6 mm, respectively, for a freestream velocity of 20 m/s or a frictional Reynolds number of $Re_\tau = u_\tau \delta/\nu = 1270$, where u_τ is the friction velocity, δ is the boundary layer thickness, and ν is the kinematic viscosity of the flow). Although all design parameters shown in Fig. 1 can potentially affect the drag performance of the array, no systematic study of the effect of these parameters on drag performance has been presented in the literature.

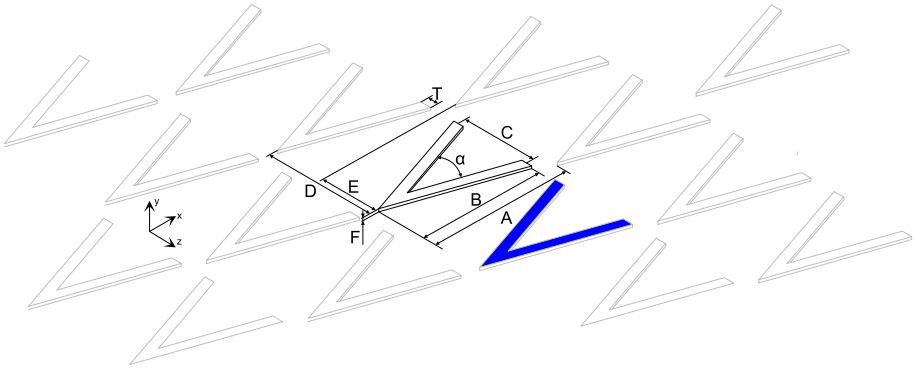

Fig. 1 Isometric view of an array of CSP with relevant design parameters: **A** is separation between rows, **B** is length of an element, **C** is width of an element, **D** is separation between elements in span, **E** is offset between rows in streamwise direction, **F** is element height, **T** is thickness of chevron legs, and $\boldsymbol{\alpha}$ is apex angle. The plan-view area of a single chevron-shape protrusion is shown in blue

According to Sirovich and Karlsson (1997), the parameter with the most drastic effect on the drag performance is the offset between rows; when the elements are aligned (i.e., zero offset), the drag increases and for a random or a constant offset, the drag is reduced.

Sirovich and Karlsson (1997) present a hypothesis for the working mechanism of this inner-scaled passive flow control technique, that is envisioned to scale with the near-wall length scale $\delta_\nu = \nu/u_\tau$. According to Sirovich and Karlsson (1997), when arranged with random offset values, the protrusions create disturbances in the flow that interact with the energetic near-wall streaks. This interaction interrupts the near-wall cycle, attenuating momentum transfer near the wall and, as a result, reducing the drag. However, there is no experimental evidence in the literature to support this hypothesis.

The proposed working mechanism builds on the principle of phase randomisation that has been shown to reduce drag in numerical simulations (Murakami et al. 1992; Handler et al. 1993) by interacting with the low-energy propagating modes presented in Sirovich et al. (1990) and Sirovich et al. (1991). A series of flow control techniques based on the principle of phase randomization were patented, utilizing various active and passive actuators (Sirovich et al. 1993; Sirovich and Levich 1993; Sirovich et al. 1994, 1997; Sirovich et al. 1998a, b, c).

Among these techniques, the CSP patented by Sirovich et al. (1998b), demonstrated sustained drag reduction of 10% over a wide range of Reynolds numbers in a channel flow using an array of protrusions with random offset, as reported by Sirovich and Karlsson (1997). In a subsequent study, Monti et al. (2001) tested CSP in an external turbulent boundary layer. The results showed a drag reduction of up to 30% for a narrow range of Reynolds numbers. However, Sagong et al. (2008) were not able to observe any drag reduction for an identical protrusion geometry. Instead, they report a drag increase between 5% and 10%. In summary, there is no consensus on the drag performance of CSP.

This study is motivated by several factors. First, there is a lack of agreement on the drag performance of CSP. Second, the effect of design parameters on the performance of the flow control technique is largely unexplored. Finally, there is no evidence to support the drag reduction mechanism postulated in the literature.

This article is structured as follows: first, the methodology is explained in Sect. 2. Experimental results are presented and discussed in Sect. 3, after which the concluding remarks and recommendations for future research are outlined in Sect. 4.

2 Methodology

The wind tunnel experiments performed in this study included direct force measurements and particle image velocimetry (PIV). In this section, the wind tunnel, the flow measurement techniques, and the protrusion test specimen designs are detailed.

2.1 Facility

The experiments were conducted in the M-tunnel at the Delft University of Technology. This tunnel was operated in an open-circuit configuration to allow for measurements in the range of $430 < Re_\tau < 1950$ at a freestream velocity of 5 m/s $< U_\infty <$ 34 m/s with a freestream turbulence intensity ($TI = u_{rms}/U_\infty$) of approximately $TI = 0.7\%$, and a test section with a constant cross-sectional area of 400 mm × 400 mm. The fixed parallel walls of the wind tunnel test section lead to a mild favorable pressure gradient over the test plate.

The boundary layer was tripped 600 mm upstream of the leading edge of the test plate ($x = -600$ mm) by means of carborundum roughness elements (grit size 24). The leading edge of the test plate is located at $x = 0$ mm (at $U_\infty = 20$ m/s: $\delta_\nu \approx 17$ μm and $u_\tau \approx 0.88$ m/s) and the trailing edge is located at $x = 881.3$ mm (at $U_\infty = 20$ m/s: $\delta_\nu \approx 18$ μm and $u_\tau \approx 0.82$ m/s). For the design of the test plates, the near-wall length scale δ_ν at the centre of the plate for the freestream velocity of 20 m/s ($Re_\tau = 1270$) was chosen and determined to be $\delta_\nu = 18$ μm using experimental data for the selected setup. The values for friction velocity u_τ and boundary layer thickness δ where also considered at the centre of the test plate for the friction Reynolds number calculation.

2.2 Direct Force Measurements

Wall-drag measurements were conducted with the balance system described in van Nesselrooij et al. (2022), which is illustrated in Fig. 2. In this article, drag is defined as the total streamwise aerodynamic force acting on the test plate, thus including the streamwise components of the tangential viscous stresses and wall-normal pressure. The dimensions of the main element of the measurement system were 1020 mm × 395 mm × 30 mm. The base (item (c) in Fig. 2) was connected through four flexures (item (e) in Fig. 2) with a connector frame (item (b) in Fig. 2) which held a test plate with dimensions 881.3 mm × 366.3 mm × 5 mm. This connector frame serves as a consistent interface between the base of the balance and the freely moving test plate; it eliminates the effect of test plate production variance ensuring a precise alignment of the test plate. The flexures allowed for the free movement of the test plate and connector in the direction of the freestream flow. The base also accommodated the ±2 N force sensor (item (j) in Fig. 2) to measure the force on the test plate. The pressure was measured at 15 locations (item (f) in Fig. 2) in the gap between the connector tray and the stationary base to correct for the force that this pressure distribution created on the test plate assembly. Furthermore, a pitot tube (item (m) in Fig. 2) was included to obtain the freestream flow velocity. A detailed description of this device, its validation, and the measurement methodology is provided in van Nesselrooij et al. (2022).

To quantify the drag reduction, drag force differences were measured relative to a smooth reference plate and expressed as the fractional drag coefficient, $\Delta C_D[\%]$:

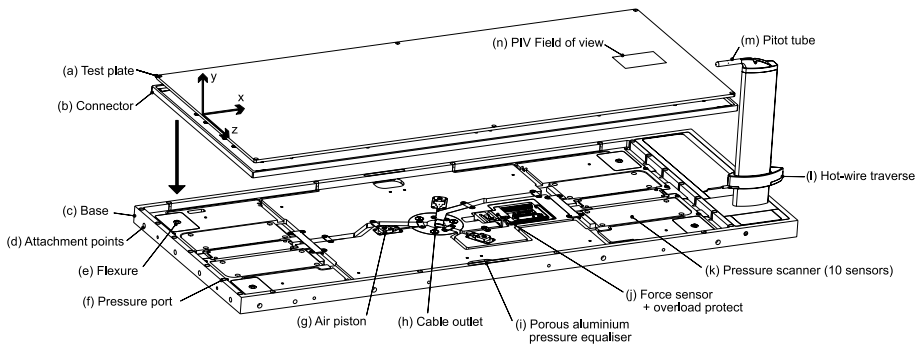

Fig. 2 Illustration of the components of the measurement system and the axis coordinate system. Modified from van Nesselrooij et al. (2022) under the terms of the Creative Commons Attribution 4.0 license

$$\Delta C_D[\%] = \frac{C_{D,\mathrm{TS}}}{C_{D,\mathrm{Ref}}} - 1,$$

where $C_{D,\mathrm{TS}}$ is the drag coefficient of the test specimen and $C_{D,\mathrm{Ref}}$ is the drag coefficient of a smooth reference plate, both tested at matching conditions. At the 95% confidence interval, the uncertainty of the balance device was less than 0.5% of the corrected drag coefficient C_D at Re_τ above 1700. Results shared in this article were taken as the average of three repeated measurements for each individual test specimen following the method of van Nesselrooij et al. (2022). To account for the drag variation of the test plates on which the protrusions were to be mounted (see Sect. 2.4), the drag forces of five randomly selected plates were measured. The variation was approximately $\Delta C_D[\%] = 1\%$ for $Re_\tau = 1700$, and this value was used throughout this study as the uncertainty of the balance measurement data. This variability is attributed to slight manufacturing differences in the shape and dimensions of the test plates.

2.3 Particle Image Velocimetry

Two dimensional-two component (2D–2C) PIV measurements were performed at a wall-parallel (x-z)-plane with a field of view of 76.4 mm × 49.4 mm. The field of view was located at 766 mm $< x <$ 842.4 mm and −17.4 mm $< z <$ 32 mm, and the location is depicted in Fig. 2. For $Re_\tau = 430$, the laser sheet was located at approximately $11.0 < y^+ < 21.7$. This wall-normal distance was estimated for the smooth reference plate from the mean streamwise velocity in the field using experimental velocity profiles for the chosen configuration. The test plate arrangement inside the wind tunnel was identical to the one described in Sect. 2.2.

Tracer particles were introduced into the flow with a SAFEX Fog 2010+ fog generator located at the wind tunnel inlet. The resulting water-glycol droplets with diameter of 1 μm were illuminated with a double-pulsed ND:Yag Evergreen 200 laser. An Imager sCMOS CLHS digital camera was used to record the particle images. Table 1 contains the illumination and imaging conditions.

The raw particle images were pre-processed using a Butterworth high-pass filter with a length of seven images to eliminate reflections before performing a multi-pass cross-correlation analysis with a final window size of 16 × 16 pixels and 75% overlap, resulting in a

Table 1 Illumination and imaging conditions for the PIV measurements

Sheet thickness dy [mm]	0.75
Pulse repetition rate [Hz]	15
Laser power [%]	60
Camera resolution [px^2]	2560 × 2160
Objective focal length f [mm]	105
Numerical aperture $f_\#$ [–]	8
Exposure [μs]	15
Scale factor [px/mm]	33.53
Field of view [mm^2]	76.35 × 49.39
Vector pitch [mm]	0.12
Vector pitch [δ_v]	6.67
Image pairs [–]	600

final vector spacing of 0.12 mm and a resolution based on the interrogation window size of $\Delta x = 0.48$ mm ($\Delta x^+ = 26.5$).

A statistical analysis was performed on the obtained velocity vector fields to compute various statistical parameters, including the mean, standard deviation, and variance. These velocity vector fields were also utilized for further analysis, such as for two-point statistics, which is a commonly used technique for characterizing the degree and size of coherent structures present within flow fields. For example, in Sillero et al. (2014), the two-point correlation analysis was applied to DNS data to characterize three-dimensional spatial correlations in a zero-pressure-gradient boundary layer, providing insights into the organization of turbulent structures and validating existing models and theories. Based on the zero-mean instantaneous fields of the streamwise velocity $u(x, z)$, the two-point correlation is defined as:

$$R_{uu}(\Delta x, \Delta z) = \frac{\overline{u(x,z)u(x+\Delta x, z+\Delta z)}}{\overline{u^2}}$$

In Fig. 3, a typical instantaneous velocity field, mean velocity field, and two-point correlation are shown for the smooth reference plate at $Re_\tau = 430$. Following the correlation factor of 0.1 px proposed by Raffel et al. (2018), the relative uncertainty of the instantaneous streamwise velocity fields was 1.38% at $Re_\tau = 430$. The uncertainty of the statistical quantities has been defined following Sciacchitano and Wieneke (2016): $\epsilon_{\overline{u}} = 0.0236$ m/s, $\epsilon_{\sigma(u)} = 0.0167$ m/s, and $\epsilon_{\sigma(u)^2} = 0.0194$ m^2/s^2 at $Re_\tau = 430$.

2.4 Test Specimen Design

The test specimens were manufactured by applying vinyl foil cut in the corresponding array design to aluminium test plates of 881.3 mm × 366.3 mm × 5 mm. The vinyl foil was Metamark 7 Series Black Matt (M7-111 M), and it was cut to shape with a Jaguar V LX 61 vinyl cutter from GCC. Except for the height (F in Fig. 1), which was fixed by the approximately 100 μm thick vinyl foil, the remaining seven design parameters shown in Fig. 1 were varied and combined in 23 unique designs. These designs were intended to make it possible to understand the effect of different parameters on the drag performance of the arrays of protrusions in addition to replicating designs from the literature. The parameters corresponding to the individual designs are presented in Table 2.

Three sets of designs were considered in this study. Firstly, the 'literature replication' set, which involved replicating experiments found in the literature. A distinction was

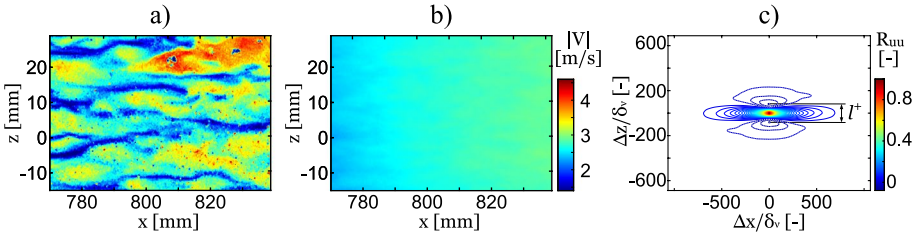

Fig. 3 Smooth reference plate at $Re_\tau = 430$ and a wall-normal distance of $y^+ = 16.37$. **a** Instantaneous flow field, **b** Mean velocity field from the average of 600 image pairs, and **c** Two-point correlation contour

Table 2 Parameters for the different designs

Design	Label	A [–]	B [–]	C [–]	D [–]	T [–]	E [–]
0	Smooth reference	N/A	N/A	N/A	N/A	N/A	N/A
1	D2 (A)	278	200	182	270	40	0
2	D2 (C)	278	200	182	270	40	135
3	Sirovich (R)$^{\triangle}$ and Sagong (40)*	300	200	200	260	40	random^{1}
4	Sirovich (A)$^{\triangle}$ and Sagong (A)*	300	200	200	260	40	0
5	Sagong (30)$^{\blacktriangle}$	300	200	200	260	30	random^{1}
6	Sagong (20)$^{\blacktriangle}$	300	200	200	260	20	random^{1}
7	Deltas (R)	300	200	200	260	40	random^{1}
8	Deltas (A)	300	200	200	260	40	0
9	D2 Patent (R)$^{\square}$	278	200	182	270	40	random^{1}
10	D3 Patent$^{\square}$	730	300	250	394	40	0
11	A = 400VU	400	200	200	260	40	random^{1}
12	A = 350VU	350	200	200	260	40	random^{1}
13	A = 230VU	230	200	200	260	40	random^{1}
14	Cavities (R)	300	200	200	260	40	random^{1}
15	Cavities (A)	300	200	200	260	40	0
16	Sirovich (R2)	300	200	200	260	40	random^{2}
17	Sirovich (R3)	300	200	200	260	40	random^{3}
18	D2 (R2)	278	200	182	270	40	random^{4}
19	Monti (A)	300	200	180	260	30	0
20	Monti (R)$^{\blacksquare}$	300	200	180	260	30	random^{5}
21	D = 400VU	300	200	200	400	40	random^{1}
22	D = 300VU	300	200	200	300	40	random^{1}
23	D = 350VU	300	200	200	350	40	random^{1}

Dimensions are normalised by near-wall length scale ($\delta_v = 18\ \mu$m). '$^{\triangle}$': designs from Sirovich and Karlsson (1997), '$^{\square}$': designs from Sirovich et al. (1998b), '$^{\blacksquare}$': design from Monti et al. (2001), '$^{\blacktriangle}$': designs from Sagong et al. (2008), '*': the same design was used in Sirovich and Karlsson (1997) and Sagong et al. (2008) at two different Reynolds numbers. Random values denoted with '^{1}' were obtained from a standard normal distribution, '^{2}' was a different set obtained in the same manner as '^{1}', '^{3}' were obtained from a uniform distribution, '^{4}' was a different set obtained in the same manner as '^{3}', and '^{5}' were chosen to match the distribution given by Monti et al. (2001)

made between aligned and random arrays of protrusions. Secondly, the 'dimensional variation' set, where parameters such as the separation between rows (A), the separation between elements in span (D), and the chevron leg thickness (T) were varied over a wide range. And thirdly, the 'morphological variation' set, where the use of deltas instead of CSP, the use of cavities instead of protrusions, and the effect of different types of offsets were analysed. The latter two sets can be grouped as 'protrusion array design parameters'. The drag performance of all designs was assessed. A sketch of a chevron, a delta, a protrusion, and a cavity is provided in Fig. 4. Additionally four designs were selected to be investigated by means of PIV to test the validity of the working mechanism proposed by Sirovich and Karlsson (1997). An overview of the designs that are included in each set is shown in Table 3.

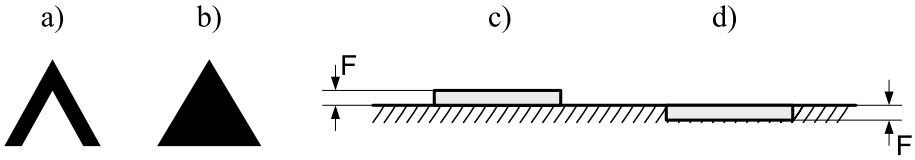

Fig. 4 Explanatory sketch of morphological variation parameters. **a** Chevron, **b** Delta **c** Protrusion of a chevron or delta, and **d** Cavity of a protrusion or delta

Table 3 Testing sets for the different designs and designs selected for PIV

Design number	1	2	3	4	5	6	7	8	9	10	11	12	13	14	15	16	17	18	19	20	21	22	23
Replication - Aligned				■						■													
Replication - Random			■		■	■			■											■			
Numerical - A			■								■	■	■										
Numerical - D			■																		■	■	■
Numerical - T				■	■	■																	
Categorical - Delta			■	■			■	■															
Categorical - Cavities			■	■										■	■								
Categorical - Offset	■	■	■	■					■							■	■	■	■	■			
PIV			■	■			■	■															

The rows indicate the testing set, and the columns indicate the design numbers. For example, for the testing set 'Replication - Aligned', the drag results for designs number 4 and 10 were relevant

To ensure that the testing was feasible within the available manufacturing resources, certain parameters introduced in Fig. 1 were held constant. Specifically, the length (B), width (C), and height (F) of the elements were kept constant, assuming that the distribution of the CSP had a greater influence on performance than their size (in the case of B and C) or manufacturing constraints (in the case of F), as previously discussed. However, an exception to this general rule is the thickness of the chevron legs (T), which was varied. This parameter has not been defined in the early literature, which motivated its inclusion in this study. In addition, the use of delta-shaped protrusions is explored as a logical derivative of CSP that offers advantages in manufacturing. Cavities are tested as an alternative design, which was suggested by Sirovich et al. (1998b), but has not been reported in previous studies.

3 Experimental Results and Discussion

In this section, the drag results obtained for the replication test cases and the design parameter study are presented and discussed. For a smaller subset of test cases selected after the drag measurements, PIV results in the form of two-point statistical data and turbulence energy levels are shared to link the drag reduction mechanism proposed by Sirovich and Karlsson (1997) to changes in the statistics of the near-wall turbulence.

3.1 Replication of Previous Studies

A summary of the drag results for the replication experiments is shown in Fig. 5. The nine results presented in this figure are divided into two groups: aligned arrays (left-most three results) and random arrays (right-most six results).

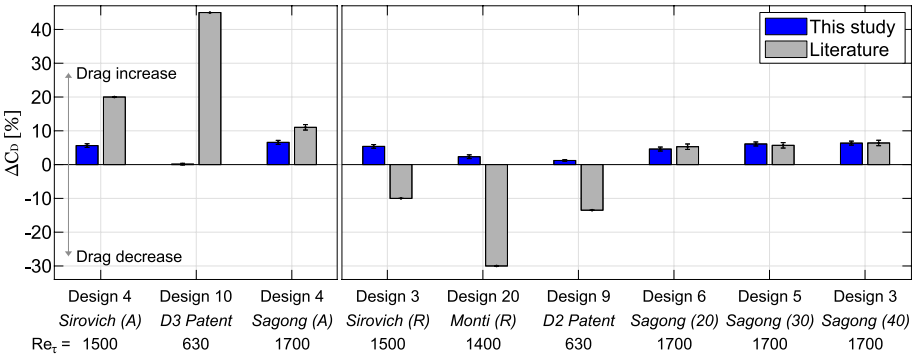

Fig. 5 Replication test case results for aligned (left) and random (right) array designs. The corresponding Reynolds numbers are indicated in the figure. Literature values were obtained from Sirovich and Karlsson (1997) (Sirovich), Sirovich et al. (1998b) (D3 and D2 Patent), Monti et al. (2001) (Monti), and Sagong et al. (2008) (Sagong). Error bars for the literature data is based on the error bars as provided in the reference literature

Not all results from previous studies were replicated. Notably, discrepancies were observed for designs 3 (at $Re_\tau = 1500$), 20, and 9, which yielded a small to moderate increase in drag instead of the drag reduction reported in the literature. The only results that showed agreement with the literature were the results by Sagong et al. (2008), particularly the random designs 6, 5, and 3 (at $Re_\tau = 1700$). Overall, no previous result for drag reduction was replicated successfully in the present investigation.

Differences in experimental methodologies could cause the discrepancies observed in the replication study. Table 4 summarises the testing conditions for all experiments from which the results were taken for the replication study. In line with the obtained results, the conditions in the study by Sagong et al. (2008) and in this study were similar; both used the same type of wind tunnel with a comparable cross section, model size, and measurement technique. Notable differences with experiments by Sirovich and Karlsson (1997), Sirovich et al. (1998b), and Monti et al. (2001) were longer test sections, larger areas covered with protrusions, and the use of pressure measurements to determine the drag force. Moreover, Sirovich and Karlsson (1997) and Sirovich et al. (1998b) performed measurements in a channel flow configuration whereas other studies tested in external flows. Although the CSP were matched in terms of their viscous scaled size, it is worth noting that there were still differences in the Reynolds numbers between the studies.

The measurement techniques used in the different studies should, when performed adequately, be expected to give comparable results. Hence, the differences in test section type (channel versus external flow), test section size, and model size are considered to be the most likely causes of the observed discrepancies in the replication test. However, the authors have no explanation for how these differences led to such discrepancies and recommend further replication studies with more identical experimental boundary conditions.

3.2 Effect of Protrusion Array Design Parameters

The design parameters were classified in dimensional and morphological variation sets. The former included the separation between rows (A), the separation between elements in span (D), and the thickness of the chevron legs (T). The morphological variation included

Table 4 Testing conditions for different studies; '^{i}': wind tunnel height diverges from 400 to 420 mm to obtain a zero pressure gradient; '^{ii}': Reynolds number based on the centreline velocity (and the channel height); '^{iii}': velocity measured at the centreline; '^{iv}': with momentum thickness θ at right before the plate ($Re_\theta = U_\infty \theta / \nu$); '^{v}': using boundary layer profile measurements obtained with a probe

	Sirovich and Karlsson (1997) (Sirovich et al. 1998b)	Monti et al. (2001)	Sagong et al. (2008)	This study
Wind tunnel	Fully developed turbulent channel flow	Open circuit, downstream blower	Open circuit, suction type	Open circuit, blower upstream (M-tunnel)
Test section size (LWH)	$8500 \times 750 \times 56.8\ \text{mm}^3$	$6000 \times 300 \times 400\ \text{mm}^3$	$2000 \times 300 \times 400\ \text{mm}^3$ [i]	$1500 \times 400 \times 370\ \text{mm}^3$
Turbulence intensity	-	-	0.5% (at 20 m/s)	$\approx$ 0.7% (at 24.7 m/s)
Reynolds number and velocity range	$15,000 < Re < 40,000$[ii] $750 < Re_\tau < 2,000$ ($10,800 < Re < 18,000$[ii])	$750 < Re_\theta < 4,250$ $5 < U_{cl} < 20$ m/s[iii]	$4,400 < Re_\theta < 8,300$[iv] $15 < U_\infty < 30$ m/s	$8.25 < U_\infty < 34.5$ m/s $630 < Re_\tau < 1950$ $1390 < Re_\theta < 4700$
Measurement	Pressure drop	Von Kármán integral relation[v]	Direct force measurement	Direct force measurement
Model size (LW)	$8530 \times 750\ \text{mm}^2$	$900 \times 300\ \text{mm}^2$	$598 \times 298\ \text{mm}^2$	$881.3 \times 366.3\ \text{mm}^2$

the use of deltas or cavities instead of CSP and different values for the offset. It should be noted that the Reynolds number $Re_\tau = 1700$ was selected for the results presented in this section. This choice was motivated by the fact that the closest agreement with existing literature was achieved at this particular Reynolds number. Nevertheless, data was obtained across a broader range, specifically $630 \leq Re_\tau \leq 1950$, and the trends discussed in this section remain consistent throughout the entire range.

3.2.1 Dimensional Variation

The drag results for different values of the separation between rows (A), the separation between elements in span (D), and the thickness of the chevron legs (T) are depicted in Fig. 6. $\Delta C_D[\%]$ decreased with increasing A and D and increased with increasing T.

The plate coverage was introduced in Fig. 6 as a metric to express the percentage of the plate that was covered by protrusion elements. The plate coverage is defined as the area of the protrusion elements (as defined in Fig. 1) divided by the total plan-view area of the test plate (i.e., $881.3 \times 366.3\,\text{mm}^2$) and is expressed in percent. This metric was used as a proxy for increased pressure drag. In all three cases studied in Fig. 6, the drag results generally followed the same trend as the plate coverage: a higher degree of plate coverage corresponded to a larger increase in drag. This suggested that the protrusions acted as roughness elements, and a larger degree of roughness led to more friction drag.

3.2.2 Morphological Variation

In Fig. 7, the drag results for an array of protrusions, deltas, and cavities are shown. The use of deltas is motivated by the fact that they have a simpler but similar shape compared to chevrons, and the use of cavities is proposed by Sirovich et al. (1998b) as an alternative to protrusions. The three designs presented in Fig. 7a are based on the same random array, and only the shape of the array elements (chevron versus delta-shaped) or their realisation (protrusion versus cavity) were varied. The same is true for Fig. 7b, where the designs were based on the same aligned array. In both configurations, the protrusion and delta designs performed similarly. However, the drag was less for the cavity than its protrusion counterpart.

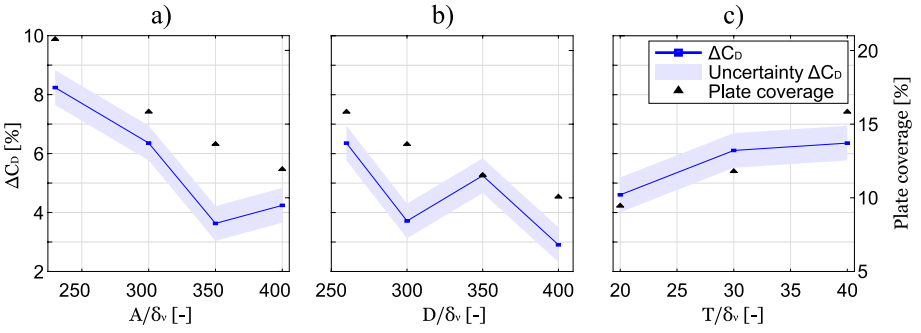

Fig. 6 Parameter sweep results for $Re_\tau = 1700$ **a** Separation between rows, **b** Separation between elements in span, and **c** Thickness chevron legs

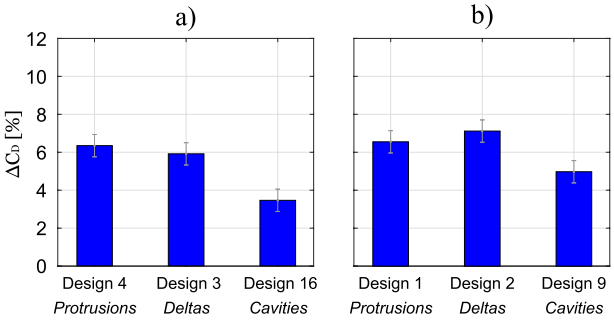

Fig. 7 Results for the delta and cavity test cases at $Re_\tau = 1700$ **a** Random array, and **b** Aligned array

The type of offset is a key parameter that according to Sirovich and Karlsson (1997) can substantially influence the drag performance. In Fig. 8, the drag results are presented for three array designs where only the offset is varied between aligned, constant, and random. The exact type of offset did not lead to a consistent difference in observed drag results. In most cases, random offsets led to a smaller increase in drag than aligned or constant offsets. However, this did not hold for designs 4 and 3 (Fig. 8a) where the aligned and random offset showed the same drag performance, and designs 2 and 9 (Fig. 8b) where the constant and a random offset led to the same increase in drag.

Considering only the random array designs (designs 3, 16, and 17 in Fig. 8a and design 9 and 18 in Fig. 8b), large differences in drag performance were observed. Arrays with offset values obtained from a uniform distribution (designs 17 and 18) had the smallest drag increase in the tested set. However, there were noticeable differences in drag performance even for designs where the random offset values were obtained using the same method, e.g., design 3 and 16 where the random offset values were obtained from a normal distribution. Furthermore, the aligned and the constant offset cases can be regarded as a special case of the random offset where the offset values are coincidentally zero or equal, respectively.

Based on the previous observations, it is possible that a set of random values could result in an even larger increase in drag than in the aligned case, while another set could lead to a smaller increase or even a decrease in drag. Therefore, further investigation is needed to focus exclusively on the effects of offset variation on drag performance.

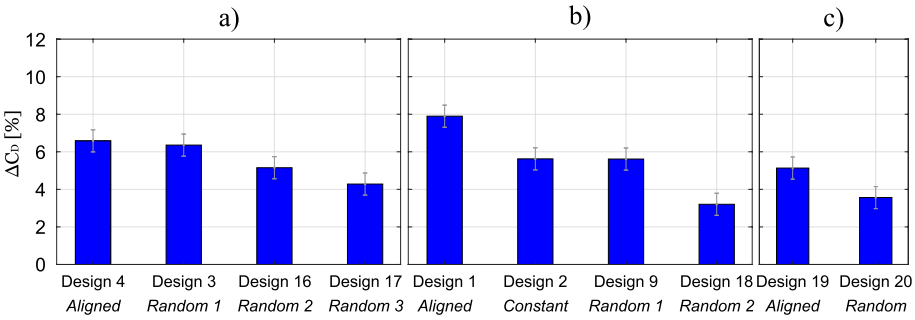

Fig. 8 Effects of different offset types and values on the drag performance at $Re_\tau = 1700$ **a** Variations from the design by Sirovich and Karlsson (1997), **b** Variations from the design by Sirovich et al. (1998b), and **c** Variations from the design by Monti et al. (2001)

3.3 Flow Structures

The flow structures were analysed for the smooth reference plate, design 3, and design 4. Designs 3 and 4 were identical except for their offsets, which were random and aligned, respectively. According to Sirovich and Karlsson (1997), this led to a large difference in the drag performance: 10% drag reduction was reported in the literature for the random array, and 20% drag increase for the aligned design. Following the hypothesis presented by Sirovich and Karlsson (1997), this difference in array configuration should be visible in the flow structures: the prevalence of low-speed streaks is hypothesised to be less pronounced for the drag reducing random array design compared to those for the drag increasing aligned array design.

3.3.1 Low-Speed Streak Spacing

A statistical spacing of the low-speed streaks can be defined with the aid of the two-point correlation maps, such as the one that was presented in Fig. 3c. A spanwise spacing (l^+) is taken as the spanwise distance between the two correlation valleys, as shown in Fig. 3c. For three designs (i.e., the smooth reference plate, design 3, and design 4), spanwise spacing values are presented in Fig. 9. As shown in Fig. 9a, the low-speed streak spacing of the smooth reference plate was larger compared to the reference data by Chernyshenko and Baig (2005). However, it is important to note that the absolute value holds secondary importance in this analysis, as the primary focus lies on assessing the increase or decrease in streak spacing.

The measurements in the three test cases were taken at different laser sheet wall-normal locations ($y^+ = 16.37$, 16.57, and 16.58). To remove this effect, the difference with respect to the reference GOP data by Chernyshenko and Baig (2005) at the corresponding normalised wall distance instead of the absolute spacing was considered for the comparison between test cases. These values are shown in Fig. 9b for the three test cases. The low-speed streak spacing difference (Δl^+) was larger for the test cases with protrusions than for the smooth plate. Hence, the protrusions affected the flow in a manner that measurably influenced the periodicity of the coherent structures in the near-wall region. However, the

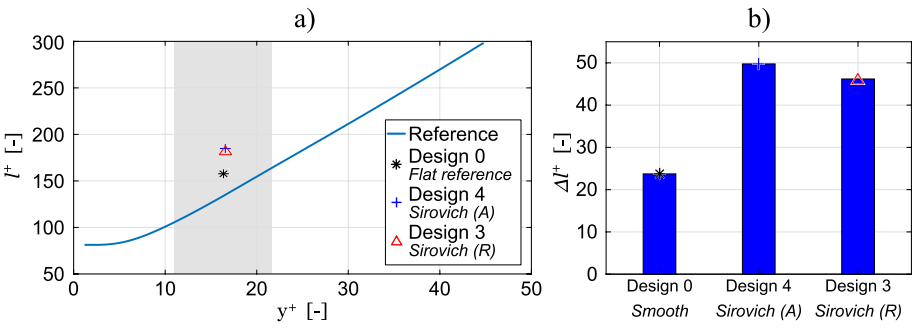

Fig. 9 **a** Normalised low-speed streak spanwise spacing (l^+) as a function of wall-normal distance for reference generalised optimal perturbation (GOP) data and the PIV test cases. GOP data at $Re = 180$ (based on the dynamic velocity and the channel half-width) from Chernyshenko and Baig (2005). Measurement data points at $Re_\tau = 430$. Grey area represents the range of the laser sheet for the smooth reference plate measurement. **b** Difference in normalised low-speed streak spanwise spacing (Δl^+) between the GOP data and the PIV test cases

spacing difference Δl^+ was similar for the random and for the aligned designs. Hence, there was no indication of fundamentally different flow structures between these two designs. Overall, these results did not support the hypothesis put forward by Sirovich and Karlsson (1997).

Furthermore, the similarity in spacing difference between designs 3 and 4, as shown in Fig. 9b, is consistent with the similar drag performance between aligned and random arrays, as observed in the direct force measurements.

3.3.2 Turbulent Kinetic Energy

The turbulence kinetic energy was examined for the same design cases as in the spanwise streak-spacing analysis to investigate whether the presence of protrusions affected the strength of coherent structures in the turbulent boundary layer.

The normalised variance of the streamwise velocity fluctuations for the three test cases and direct numerical simulation (DNS) reference data by Schlatter and Örlü (2010) are shown in Fig. 10a. The experimental data have a consistently smaller variance than the reference data. This was a result of the limited resolution of the PIV experiments, which failed to capture the energy of the subresolution turbulent scales and hence underestimated the total turbulence kinetic energy, as opposed to DNS, where all scales are resolved. Given that the attenuation remains consistent across all PIV test cases, the available data is deemed adequate for conducting a qualitative comparison among these cases.

In the same manner as presented in Sect. 3.3.1, the inaccuracy introduced by the different laser sheet wall-normal location for the three PIV test cases was corrected by considering the difference between the experimental value and the DNS reference value at the same y^+ wall-normal location. The resulting differences in variance for the smooth test plate, design 3, and design 4 were presented in Fig. 10b. As shown in this figure, the difference in variance was smaller for the designs with protrusions than for the smooth reference plate (note the negative axis); hence, the introduction of protrusions reduced the strength of the velocity fluctuations.

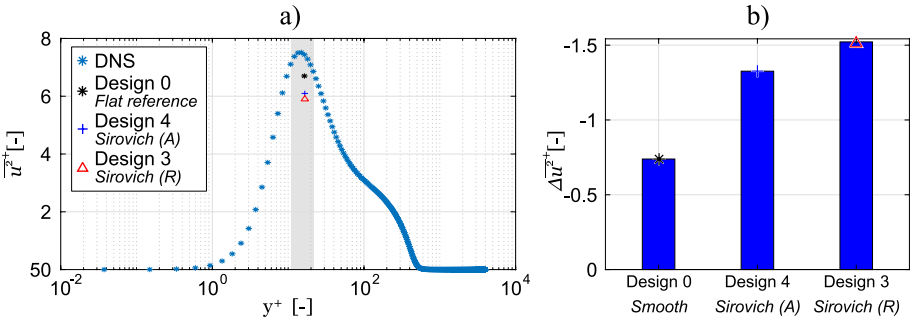

Fig. 10 **a** Normalised variance of the streamwise velocity fluctuation ($\overline{u^2}^+$) as a function of wall-normal distance for DNS data and the PIV test cases. DNS data at $Re_\tau = 492$ from Schlatter and Örlü (2010). Measurement data points at $Re_\tau = 430$. Grey area represents the range of the laser sheet for the reference measurement. **b** Difference in normalised variance of the streamwise velocity fluctuation ($\Delta\overline{u^2}^+$) between the DNS data and the PIV test cases

This reduction in turbulence energy did not match the drag balance data, which showed a drag increase for both protrusion designs. Since the measurement data points were in the area of the variance peak, a small offset in the laser wall-normal location y^+ could have been responsible for this incongruence. Two sources that can explain the offset in y^+ are a wrong estimation of the actual wall-normal location of the laser sheet and the fact that the flow might have perceived a different 'equivalent wall' due to the presence of the protrusion elements. For a qualitative comparison, the available data for the aligned and the random arrays are considered adequate since both have a very similar mean velocity (0.47% difference) and, hence, are representative of the same y^+ distance from the wall.

If the difference in variance compared to the smooth reference plate was larger for the aligned array and smaller for the random array, then the results could be interpreted as evidence to support the strengthening or weakening of the structures with respect to the smooth design hypothesis by Sirovich and Karlsson (1997). However, this trend could not be observed in Fig. 10b, where the differences in variance for both protrusion arrays were smaller than for the smooth reference plate. Hence, no distinction could be observed between the aligned and the random arrays that would indicate fundamentally different flow characteristics.

4 Concluding Remarks

CSP as a drag reducing flow control technique were studied using direct force measurements and PIV to address the current lack of agreement on their effects on drag, to understand the effects of different design parameters on their drag performance, and to find experimental evidence to assess a current hypothesis about their working mechanism. In the configurations and within the design space considered in this study, no drag reduction was observed for arrays of protrusions.

The drag reduction reported by Sirovich and Karlsson (1997), Sirovich et al. (1998b), and Monti et al. (2001) could not be reproduced in this study. However, the drag increase reported by Sagong et al. (2008) was reproduced. Substantial differences were observed between the methodologies of the studies that reported a drag reduction (i.e., Sirovich and Karlsson (1997); Sirovich et al. (1998b), and Monti et al. (2001)) and those that reported a drag increase (i.e., Sagong et al. (2008) and this study). However, the current understanding of the drag reduction mechanism would not have predicted this discrepancy. Thus, the theoretical working principle of CSP appears to be incomplete or misleading.

The large investigation of parametric effects performed in this study resulted in the salient finding that the drag performance was highly dependent on the offset values between rows. The separation between rows, separation between elements in span, and thickness of the chevron legs affected the drag performance in a manner similar to that of the plate coverage, which may have been associated with increased pressure drag. Furthermore, chevrons and delta shapes had similar drag performance, and the increase in drag was smaller for cavities than protrusions, all other design parameters being equal.

The analysis of the low-speed streak spacing showed similar results for random and aligned arrays, which was consistent with the drag data obtained in this study. The analysis of the variance showed a reduction in turbulence energy when protrusions were used, which did not coincide with the trend from the drag data. Furthermore, both the low-speed streak spacing and the variance values did not provide evidence to support the working hypothesis presented by Sirovich and Karlsson (1997).

Although no drag reduction was observed in this study, further efforts to replicate the results by Sirovich and Karlsson (1997) are deemed worthwhile due to the expected practical value of this technology. For example, future studies of CSP in a channel flow could help to further understand the underlying flow physics and to confirm the validity of the near-wall length scale to scale the CSP, or studies that focus on the offset parameter could quantify the extent to which this can affect the drag performance. A recommendation is made for configurations that demonstrate drag reduction to undergo a thorough analysis of velocity and turbulence intensity profiles, energy spectra, and large-scale features, similar to the studies conducted by Nugroho et al. (2013) and Harun et al. (2020).

Acknowledgements The authors kindly thank Dr. A.F. Rius Vidales for assisting in the PIV experiments and N.P.J. Verdegaal for his support with the direct force measurements.

Author Contributions J. Carrasco Grau: Conceptualization; Formal Analysis; Investigation; Writing—original draft. O.W.G. van Campenhout: Conceptualization; Funding acquisition; Writing—review and editing. F.H. Hartog: Investigation; Writing—review and editing. M. van Nesselrooij: Funding acquisition; Methodology; Writing—review and editing. W.J. Baars: Supervision; Writing—review and editing. F.F.J. Schrijer: Supervision; Writing—review and editing.

Funding This work was supported by the Netherlands Enterprise Agency under Grant Number TSH21002.

Declarations

Conflict of interest The authors O.W.G. van Campenhout, F.H. Hartog, and M. van Nesselrooij own stock in the company Dimple Aerospace B.V. and receive a salary from the company Dimple Aerospace B.V.

References

Chernyshenko, S.I., Baig, M.F.: The mechanism of streak formation in near-wall turbulence. J. Fluid Mech. **544**, 99–131 (2005). https://doi.org/10.1017/S0022112005006506

Choi, K.S.: The rough with the smooth. Nature **440**(7085), 754–754 (2006). https://doi.org/10.1038/440754a

Fransson, J.H.M., Talamelli, A., Brandt, L., et al.: Delaying transition to turbulence by a passive mechanism. Phys. Rev. Lett. **96**(6), 064,501 (2006). https://doi.org/10.1103/PhysRevLett.96.064501

Handler, R.A., Levich, E., Sirovich, L.: Drag reduction in turbulent channel flow by phase randomization. Phys. Fluids A Fluid Dyn. **5**(3), 686–694 (1993). https://doi.org/10.1063/1.858652

Harun, Z., Abbas, A.A., Lotfy, E.R., et al.: Turbulent structure effects due to ordered surface roughness. Alexandria Eng. J. **59**(6), 4301–4314 (2020). https://doi.org/10.1016/j.aej.2020.07.035

Monti, R., De Ponte, S., Levich, E.: Effects on the Resistance and on the Separation of V Shapes Passive Manipulators in a Turbulent Boundary Layer, pp. 255–267. Springer Vienna, Vienna (2001). https://doi.org/10.1007/978-3-7091-2574-8_9

Murakami, Y., Shtilman, L., Levich, E.: Reducing turbulence by phase juggling. Phys. Fluids A Fluid Dyn. **4**(8), 1776–1781 (1992). https://doi.org/10.1063/1.858399

Nugroho, B., Hutchins, N., Monty, J.P.: Large-scale spanwise periodicity in a turbulent boundary layer induced by highly ordered and directional surface roughness. Int. J. Heat Fluid Flow **41**, 90–102 (2013). https://doi.org/10.1016/j.ijheatfluidflow.2013.04.003

Raffel, M., Willert, C.E., Scarano, F., et al.: Particle Image Velocimetry: A Practical Guide. Springer (2018). https://doi.org/10.1007/978-3-319-68852-7

Rius Vidales, A.F., Kotsonis, M.: Impact of a forward-facing step on the development of crossflow instability. J. Fluid Mech. **924**, A34 (2021). https://doi.org/10.1017/jfm.2021.497

Sagong, W., Kim, C., Choi, S., et al.: Does the sailfish skin reduce the skin friction like the shark skin? Phys. Fluids **20**(10), 101,510 (2008). https://doi.org/10.1063/1.3005861

Schlatter, P., Örlü, R.: Assessment of direct numerical simulation data of turbulent boundary layers. J. Fluid Mech. **659**, 116–126 (2010). https://doi.org/10.1017/S0022112010003113

Sciacchitano, A., Wieneke, B.: PIV uncertainty propagation. Meas. Sci. Technol. **27**(8), 084,006 (2016). https://doi.org/10.1088/0957-0233/27/8/084006

Sillero, J.A., Jiménez, J., Moser, R.D.: Two-point statistics for turbulent boundary layers and channels at Reynolds numbers up to $\delta^+ \approx 2000$. Phys. Fluids **26**(10), 105,109 (2014). https://doi.org/10.1063/1.4899259

Sirovich, L., Karlsson, S.: Turbulent drag reduction by passive mechanisms. Nature **388**(6644), 753–755 (1997). https://doi.org/10.1038/41966

Sirovich, L., Levich, E.: Method of and apparatus for controlling turbulence in a wall-bounded fluid flow field. US Patent No. 5.263.793 (1993)

Sirovich, L., Ball, K.S., Keefe, L.R.: Plane waves and structures in turbulent channel flow. Phys. Fluids A Fluid Dyn. **2**(12), 2217–2226 (1990). https://doi.org/10.1063/1.857808

Sirovich, L., Ball, K.S., Handler, R.A.: Propagating structures in wall-bounded turbulent flows. Theor. Comput. Fluid Dyn. **2**(5), 307–317 (1991). https://doi.org/10.1007/BF00271470

Sirovich, L., Bronicki, L., Levich, E.: Method and apparatus for controlling turbulence in a wall-bounded fluid flow field. European Patent Office Patent No. 0 543 647 A1 (1993)

Sirovich, L., Levich, E., Bronicki, L.: Method of and apparatus for controlling turbulence in a wall-bounded fluid flow field. US Patent No. 5.362.179 (1994)

Sirovich, L., Levich, E., Bronicki, L.: Method of and apparatus for controlling turbulence in boundary layer and other wall-bounded fluid flow fields. US Patent No. 5.595.205 (1997)

Sirovich, L., Levich, E., Bronicki, L.: Method and apparatus for controlling turbulence in boundary layer and other wall-bounded fluid flow fields. US Patent No. 5.797.414 (1998a)

Sirovich, L., Levich, E., Bronicki, L., et al.: Apparatus for controlling turbulence in boundary layer and other wall-bounded fluid flow fields. US Patent No. 5.833.389 (1998b)

Sirovich, L., Levich, E., Bronicki, L., et al.: Method and apparatus for controlling turbulence in boundary layer and other wall-bounded fluid flow fields. European Patent Office Patent No. EP 0 850 832 A1 (1998c)

Spalart, P.R., McLean, J.D.: Drag reduction: enticing turbulence, and then an industry. Philos. Trans. R. Soc. A Math. Phys. Eng. Sci. **369**(1940), 1556–1569 (2011). https://doi.org/10.1098/rsta.2010.0369

Tani, I.: Drag reduction by riblet viewed as roughness problem. Proc. Jpn. Acad. Ser. B **64**(2), 21–24 (1988). https://doi.org/10.2183/pjab.64.21

van Nesselrooij, M., van Campenhout, O.W.G., van Oudheusden, B.W., et al.: Development of an experimental apparatus for flat plate drag measurements and considerations for such measurements. Meas. Sci. Technol. **33**(5), 055,303 (2022). https://doi.org/10.1088/1361-6501/ac527f

Walsh, M.: Turbulent boundary layer drag reduction using riblets. AIAA Paper, p. 169 (1982). https://doi.org/10.2514/6.1982-169